digitization rate results in a 40 □s readout gradient span.

In conclusion, the present technological innovation has enabled us to obtain good quality EEG data even under the unfavorable condition of fMRI acquisition. Accordingly, broad practical utilization of both high quality EEG and concomitant brain hemodynamic mapping through fMRI can provide a new understanding of the generating systems of various spontaneous EEG activities such as basic waves (α, β, and γ waves), epileptic spikes, and sleep hump and spindle waves, as well as those of ERP components, in terms of anatomical substrates apart from the volume conduction mechanism of electricity.

ACKNOWLDGEMENT

This study was supported by a research grant (11B-3) for Nervous and Mental Disorders from the Ministry of Health, Labour and Welfare (Japan).

APPENDIX

In the SSS method, data sampling with 1000 Hz digitization rate (Fs) with 3000 Hz of high cut-off frequency in the anti-aliasing filter (The highest frequency included in the data (Fh) = 3000 Hz) was used. Then,

$$\text{Nyquist frequency} = (1/2)*Fs < Fh$$

Accordingly, this condition violates the sampling theorem, and thus the acquired data should have aliasing contamination. The aliasing contamination is defined by the data components of which frequencies are higher than the Nyquist frequency. For estimating the aliasing contamination, human EEG data in a magnet with (B)/without (A) fMRI acquisition at 20000 Hz digitization rate with 3500 Hz high cut-off frequency of LPF in the SynAmps preamplifier were recorded. The data during fMRI acquisition were artifact-corrected with averaged artifact subtraction. In the following figure A and B, the power spectrum density of the data are demonstrated. Both EEG data had 105 $(□V)^2$ of EEG signal peaks at around 10 Hz and had less than 0.6 $(□V)^2$ of components up to

10000 Hz (Nyquist frequency of the digitization rate) except the one at 600 Hz (see the magnified figures inside. the range from 1000 Hz to 10000 Hz not shown in the figure). The underlying 600 Hz component was clearly visible and could cause substantial aliasing contamination in the data. However, the aliasing by the components at Fa Hz ranging from the Nyquist (500 Hz) to 900 Hz including the outstanding 600 Hz component can emerge at the frequency (1000 – Fa) Hz ranging from 100 Hz to 500 Hz that are higher than our interest of EEG data frequency range and thus, can be eliminated by a usual LPF procedure. Next, the actual alias contamination was estimated by EEG inspection using the above data in a magnet. Two sets of data were derived from the data using the different procedures. Alias-clean EEG was first low-pass filtered with 80 Hz and subsequently down sampled at a 1000 Hz digitization rate. Alias-contaminated EEG was first down sampled to 1000 Hz and subsequently low-pass filtered with 80 Hz, which should have alias contamination. Figure C demonstrated these alias clean/contaminated EEG data in parallel. It was found that there was no apparent difference between them with inspection. From this result, it was concluded that aliasing contamination did not substantially interfere with EEG observation during fMRI acquisition using SSS method.

REFERENCES

Allen, P.J., Polizzi, G., Krakow, K., Fish, D.R., Lemieux, L. 1998. Identification of EEG events in the MR scanner: the problem of pulse artifact and a method for its subtraction. *Neuroimage* **8**(3):229-239.

Allen, P.J., Josephs, O., Turner, R. 2000. A method for removing imaging artifact from continuous EEG recorded during functional MRI. *Neuroimage* **12**(2):230-239.

Anami, K., Saitoh, O., Yumoto, M. 2002 Reduction of ballistocardiogram with a vacuum head-fixating system during simultaneous fMRI and multi-channel monopolar EEG recording. *International Congress Series 1232, Recent Advances in Human Brain Mapping* **1232**:427-431.

Belliveau, J.W., Kennedy, D.N, Jr., McKinstry, R.C., Buchbinder, B.R., Weisskoff, R.M., Cohen,

M.S., Vevea, J.M., Brady, T.J., Rosen, B.R. 1991.

Functional mapping of the human visual cortex by magnetic resonance imaging. *Science* **254**:716-719.

Bonmassar, G., Anami, K., Ives, J., Belliveau, J.W. 1999. Visual evoked potential (VEP) measured by simultaneous 64-channel EEG and 3T fMRI. *Neuroreport* **10**(9):1893-1897.

Bonmassar, G., Schwartz, D.P., Liu, A.K., Kwong, K.K., Dale, A.M., Belliveau, J.W. 2001. Spatiotemporal brain imaging of visual-evoked activity using interleaved EEG and fMRI recordings. *Neuroimage* **13**(6 Pt 1):1035-1043.

Goldman, R.I., Stern, J.M., Engel, J, Jr., Cohen, M.S. 2000.

Acquiring simultaneous EEG and functional MRI. *Clin. Neurophysiol.* **111**(11):1974-1980.

Hoffmann, A., Jager, L., Werhahn, K.J., Jaschke, M., Noachtar, S., Reiser, M. 2000.

Electroencephalography during functional echo-planar imaging: detection of epileptic spikes using post-processing methods. *Magn. Reson. Me.d* **44**:791-798.

Krakow, K., Woermann, F.G., Symms, M.R., Allen, P.J., Lemieux, L., Barker, G.J., Duncan, J.S., Fish, D.R. 1999. EEG-triggered functional MRI of interictal epileptiform activity in patients with partial seizures. *Brain* **122** (Pt 9):1679-1688.

Kruggel, F., Wiggins, C.J., Herrmann, C.S., von Cramon, D.Y. 2000. Recording of the event-related potentials during functional MRI at 3.0 Tesla field strength. *Magn. Reson. Med.* **44**(2):277-282.

Kruggel, F., Herrmann, C.S., Wiggins, C.J., von Cramon, D.Y. 2001. Hemodynamic and electroencephalographic responses to illusory figures: recording of the evoked potentials during functional MRI. *Neuroimage* **14**(6):1327-1336.

Lazeyras, F., Blanke, O., Perrig, S., Zimine, I., Golay, X., Delavelle, J., Michel, C.M., de Tribolet, N., Villemure, J.G., Seeck, M. 2000. EEG-triggered functional MRI in patients with pharmacoresistant epilepsy. *J. Magn. Reson. Imaging* **12**(1):177-185.

Lemieux, L., Krakow, K., Fish, D.R. 2001a. Comparison of spike-triggered functional MRI BOLD

activation and EEG dipole model localization. *Neuroimage* **14**(5):1097-1104.

Lemieux, L., Salek, Haddadi, A., Josephs, O., Allen, P., Toms, N., Scott, C., Krakow, K., Turner, R., Fish, D.R. 2001b. Event-related fMRI with simultaneous and continuous EEG: description of the method and initial case report. *Neuroimage* **14**(3):780-787.

Salek, Haddadi, A., Merschhemke, M., Lemieux, L., Fish, D.R. 2002. Simultaneous EEG-Correlated Ictal fMRI. *Neuroimage* **16**:32-40.

Warach, S., Ives, J.R., Schlaug, G., Patel, M.R., Darby, D.G., Thangaraj, V., Edelman, R.R., Schomer, D.L. 1996. EEG-triggered echo-planar functional MRI in epilepsy. *Neurology* **47**(1):89-93.

LEGENDS

Fig. 1. A: Timings of RF emission and gradient pulses in an fMRI sequence (EPIS, Siemens:ep2d_fid_60b2080_62_64.ekc) RF: radio frequency wave, Gs: slice selection gradient, Gp: phase encoding gradient, Gr: readout gradient. a: Fat-Sat pulses (1-3-3-1 pulses), b: slice selection RF, c,d,h: spoilers, e: slice selection gradient, f: dephasing and rephrasing gradient g: readout gradient. *B:* Schematic diagram of whole EPIS sequence. *C:* Imaging artifact waveform for one slice scan on a dummy EEG record with a phantom using the EPIS sequence. The artifact corresponding to each gradient component described above in A can be identified and is denoted by the same alphabet with apostrophe as that denoting the original gradient.

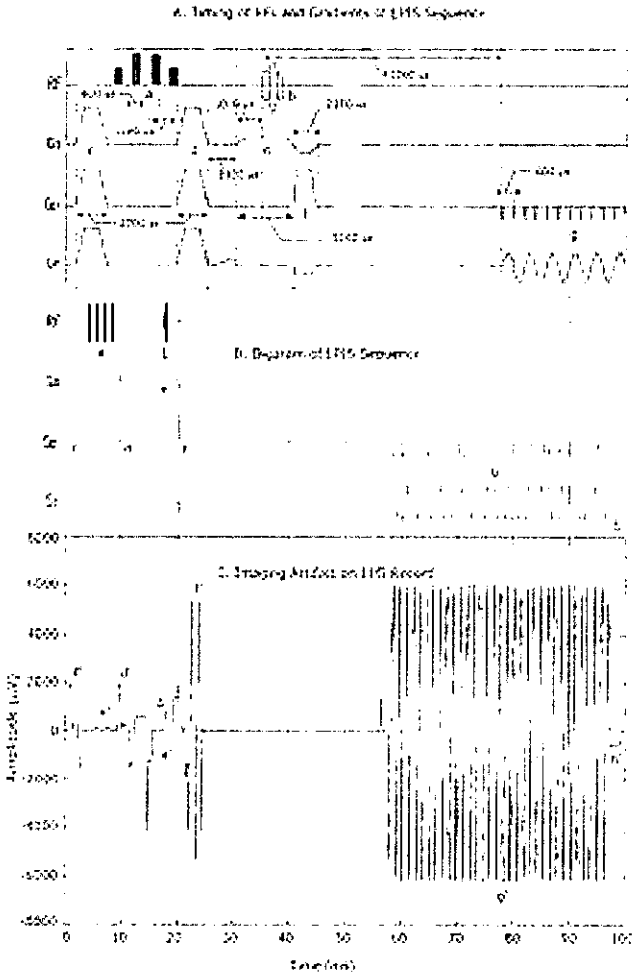

Fig.2. Electrode placement and structure. *A:* Electrode placement is based on the standard 10-20 system. *B:* each electrode has double plates inside for shielding.

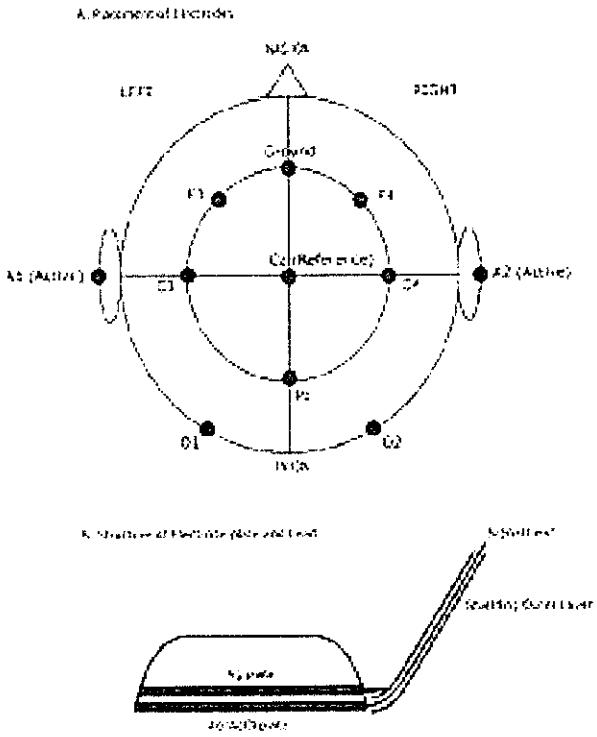

Fig. 3. Schematic diagram of the stepping stone sequence. *A:* Diagram of the series of RF and gradient pulses in the stepping stone sequence is illustrated. RF: RF pulses, Gs: slice selection gradient, Gp: phase encoding gradient, Gr: readout gradient, a: Fat-Sat pulses, b: slice selection RF, c: spoiler, d: slice selection gradient, e: dephasing and rephasing gradient, f: readout gradient : EEG sampling point with 1000Hz digitization rate *B:* An example of predicted imaging artifact waveform made by sum of the differential waveforms of the each gradient pulses (Gs, Gp, Gr). Digitally sampled dots for EEG signal (1000 Hz digitization rate) are superimposed on the artifact waveform. Every sampling point avoids artifact spikes. *C:* Magnified figure of the former part of A. Timings of RFs and gradient pulses are illustrated. *D:* Magnified figure of the readout gradient of A. 400 μs still time on the top of the readout gradient results in the sampling shelf in the imaging artifact that allows stable phase-locked EEG sampling.

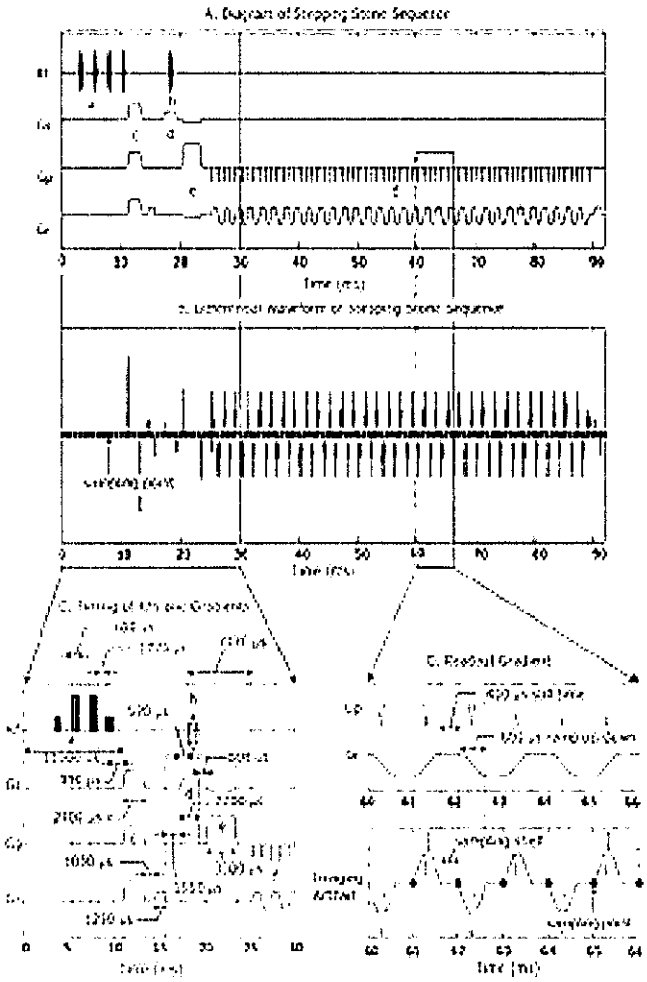

Fig.4. Activated areas in occipital lobe from the first experiment were demonstrated with the EPIS and the Stepping stone sequence. The time courses of the NMR signal with the two sequences were also demonstrated. Xm, Ym and Slm denote the coordinate and the slice number of the ROI that showed the maximum percent change in the NMR signal between the task/control blocks.

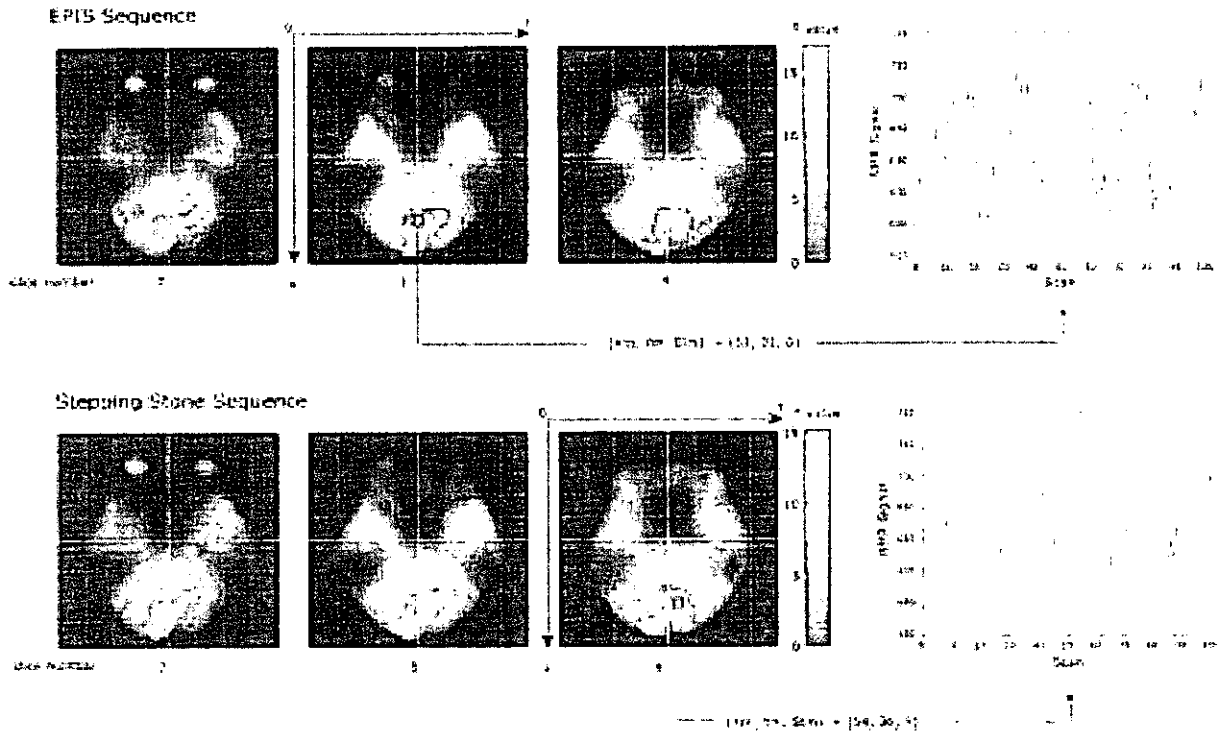

Fig. 5. Imaging artifact and residues after artifact subtraction in SSS and non-SSS acquisition. *A. Imaging Artifact:* Averaged artifact on a phantom from SSS and non-SSS acquisition in which 20 slices for one volume scan were obtained. Large series of artifact peaks are of non-SSS acquisition, whereas the smaller one is of SSS acquisition. *B. Subtracted Data:* The data during one volume scan (20 slices, 1840 ms) after averaged-artifact subtraction were illustrated in non-SSS and SSS acquisition. Background noise for the same span is also displayed for reference. *C. Spectrogram:* specgram.m program in Matlab modified to display power was used for temporal FFT analysis. Temporal FFT profiles (from DC up to 100 Hz) of subtracted data are illustrated for non-SSS and SSS, as well as imaging artifact and background noise. The color map demonstrates a power spectrum for 27 s of fMRI scans. In this color code the hotter the color the higher is the power. Weak spectral power bands observable at 50Hz and 100Hz are hum noise and its harmonics respectively.

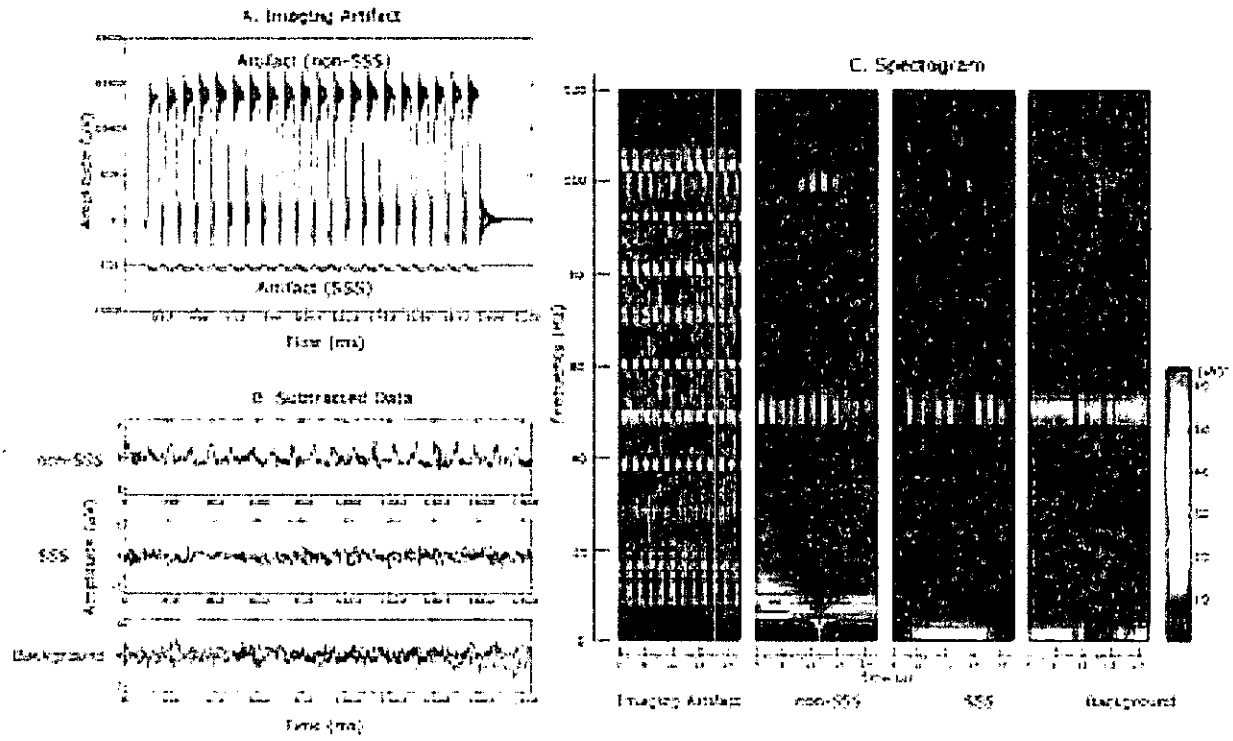

Fig. 6. Retrieved time domain EEG record during fMRI acquisition. Seven channels of retrieved EEG data referred to Cz for 10 s after artifact correction are illustrated. During the middle 2 scans, a subject closed his eyes, while he opened them within scans at both ends. α activity was augmented during eyes closed periods, while β activity was predominant during eyes opened periods.

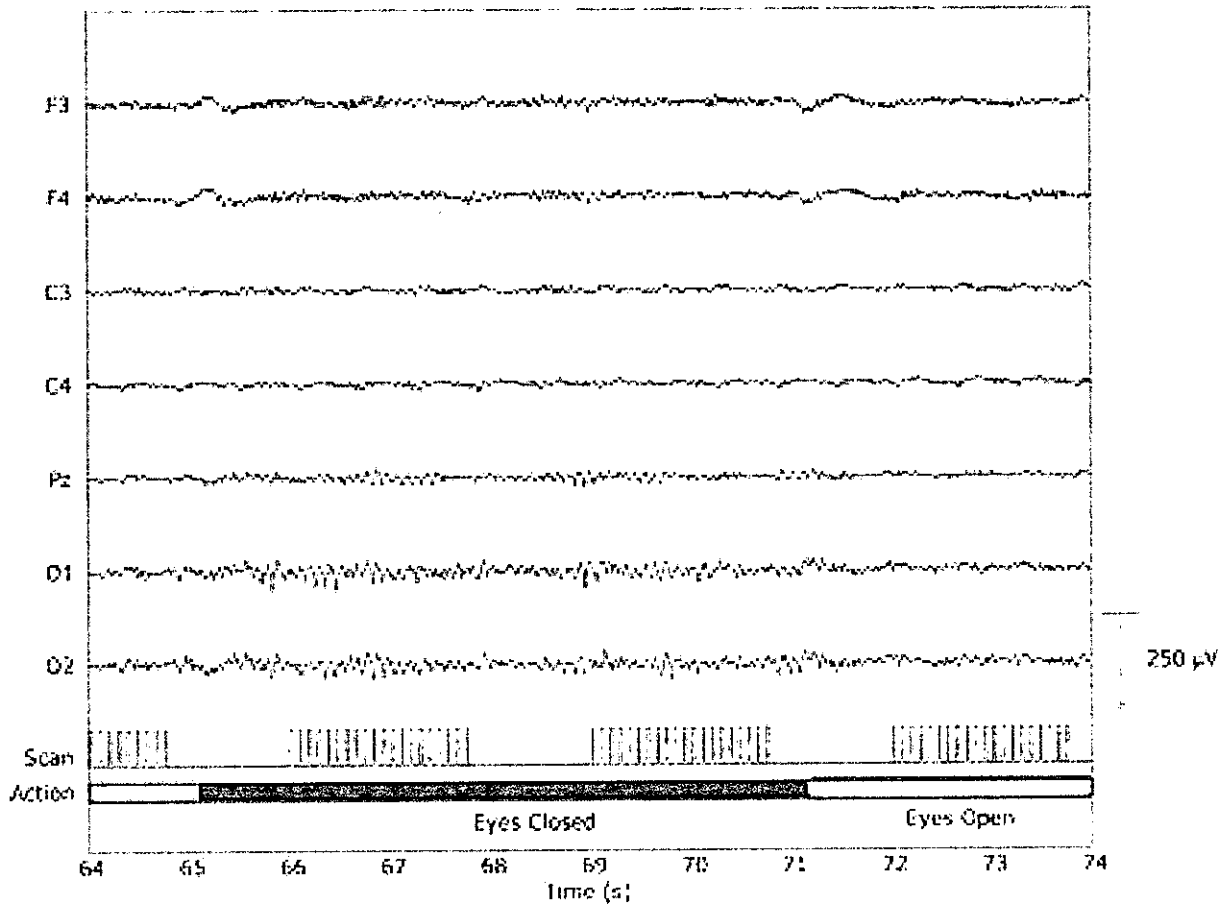

Fig. 7. Spectrogram of human EEG during 100 volumes acquisition. Temporal FFT result of the whole EEG data on O2 site of the same experiment as shown in Fig.6 is illustrated. The modified specgram.m in Matlab was used. Subject was instructed to open/close his eyes every 2 scans alternatively. The first 15 scans had no artifact correction so as to demonstrate the original artifacts. The next 85 scans were artifact-corrected. After fMRI acquisition, EEG continued to be further recorded for the next 3 min. The subject once stopped open/close eyes behavior at the end of fMRI acquisition and resumed it 1 min later. Harmonic hum noise was weakly visible around 100 Hz.

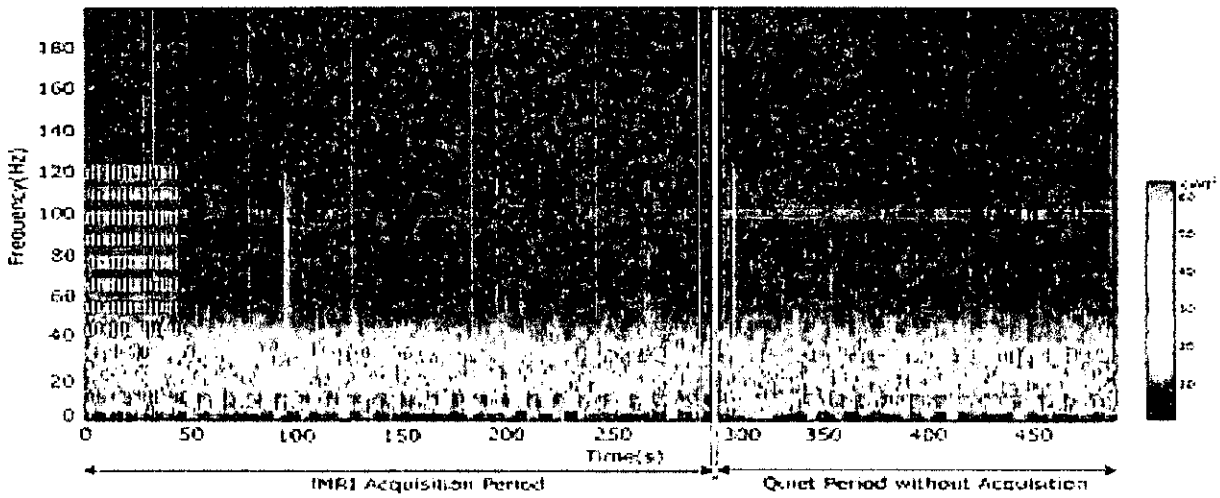
Frequency(Hz)
180
160
140
120
100
80
60
40
20
0
0
50
100
150
200
250
300
350
400
450
Time(s)
fMRI Acquisition Period
Quiet Period without Acquisition

Endogenous dopamine release induced by repetitive transcranial magnetic stimulation over the primary motor cortex: An [^{11}C] raclopride PET study in anesthetized macaque monkeys

Takashi Ohnishi 1),2), Takuya Hayashi 2), Yoshikazu Ugawa 3),
Shingo Okabe 1,3), Ikuo Nonaka 4), Hiroshi Matsuda 1),
Hidehiro Iida 2), Etsuko Imabayashi 1), Hiroshi Watabe 2),
Yoshihiro Miyake 2), Mikako Ogawa 2), Noboru Teramoto2),
Yoichirou Ohta 2), Norimasa Ejima 5)

1) Department of Radiology, National Center Hospital of Mental, Nervous and Muscular Disorders, National Center of Neurology and Psychiatry
4-1-1 Ogawa higashi, Kodaira City, Tokyo 187-8551, Japan

2) Department of Investigative Radiology, National Cardio-Vascular Center, Research Institute, 5-7-1 Fujishiro-dai, Suita, Osaka 565-8565, Japan

3) Department of Neurology, Division of Neuroscience, Graduate School of Medicine, University of Tokyo, 7-3-1 Hongo, Bunkyo-ku, Tokyo 113-8655, Japan

4)

5) Institute for Biofunctional Reserch Ltd, 5-7-1 Fujishiro-dai, Suita, Osaka 565-8565, Japan

Corresponding author: Takashi Ohnishi, 4-1-1 Ogawa Higashi, Kodaira City, Tokyo 187-8551, Japan Telephone: 81-42-341-2711 Fax: 81-42-346-1790

e-mail : tohnishi@hotmail.com

Summary: Repetitive TMS (rTMS) has been used as a potential treatment for neuropsychiatric disorders, such as depression and Parkinson's disease. Despite the growing interest in therapeutic application of rTMS, the precise mechanisms of action of rTMS are still unknown. With respect to PD, activation of the mesostriatal dopaminergic pathway is likely to be a possible candidate mechanism behind the therapeutic effects, however, modulating effects of rTMS over the M1 on the dopaminergic system have not been studied. Here we used [11C] raclopride positron emission tomograpahy to determine changes in extracellular dopamine concentration after 5Hz of rTMS over the motor cortex in seven anesthetized monkeys. rTMS over the left M1 caused a reduction of [11C] raclopride binding in the ventral striatum including the nucleus accumbens. No significant reduction of binding potential (BP) was found in the dorsal striatum but a significant increase of the BP in the right putamen was observed. These data indicate that rTMS over the motor cortex induces the release of endogenous dopamine in the ventral striatum. Our results suggest that therapeutic mechanisms of rTMS should be explained by the activation in the mesolimbic dopaminergic pathway, which plays critical roles in rewards, reinforcement and incentive motivation

Key words: PET, rTMS, depression, dopamine

Introduction

Recently, repetitive TMS (rTMS) has been investigated as a potential treatment in neuropsychiatric disorders such as depression (Pascal Leone et al., 1996, George et al., 1997, Klein et al., 1999, Berman et al., 2000), schizophrenia (George et al. 1999), and Parkinson disease (Dragasevic et al., 2002). Although the most prominent example of therapeutic rTMS is the application for depression, several investigators have applied rTMS for treatment of movement disorders, such as Parkinson's disease (PD). Pascual-Leone and colleagues (1996) first applied rTMS over the hand area of the motor cortex (M1) to the treatment of PD. Later reports have used rTMS as a potential therapeutic tool for PD and some of them showed a therapeutic effect (Mally, 1999, Siebner, 1999, Sommer 2002,), whereas others found no significant effects (Ghabra MB 1999, Tergau. 1999). In one study, rTMS over supplementary motor area (SMA) worsened motor performance (Boylan, 2001). At the present time it seems unclear whether rTMS over the M1 has a beneficial effect on PD (Wassermann EM , 2001, Cantello R 2002).

Further, the precise therapeutic mechanisms of rTMS have been still unclear.

Several investigations suggested that the local effects similar to long-term depression and long-term potential and distant effects in functionally connected areas to stimulated site should explain therapeutic mechanisms of rTMS (George et al., 1995, Kimbrel et al., 1999, George et al., 1999a, 199b, Nahas et al., 2001a, 2001b, Kimbrel et al., 2002). On the other hand, animal studies have indicated that rTMS induces attenuation of the hypothalamic-pituitary-adrenocortical system suggesting regional changes neurotransmitter release and transsynaptic efficiency (Keck et al., 2000,2001).

The dopaminergic system is one of candidate neurotransmitter systems considered to be associated with therapeutic mechanisms of rTMS. A human PET study and animal studies using microdialysis indicated that rTMS over the frontal cortex has modulating effects on the dopaminergic system (Keck et al., 2002, Strafellea, et al. 2001). With respect to PD, activation of the mesostriatal dopaminergic pathway is likely to be a possible candidate mechanism behind the therapeutic effects of rTMS, however, modulating effects of rTMS over the M1 on the dopaminergic system have not been studied. The aim of the present study is to use positron emission tomograpahy (PET) to determine whether rTMS over the M1 induces dopamine release in the striatum of the monkey brain and where such modulating effects are found.

Methods and Materials

Experimental design

Young-adult male cynomolgous monkeys (*macaca fascicularis*; n=8) weighing from 4.7 to 5.0 kg were used for the PET measurements. Monkeys were maintained and handled in accordance with guidelines for animal research on Human Care and Use of Laboratory Animals (Rockville, National Institute of Health/Office for Protection from Research Risks, 1996). The study was also approved by the ethical committee for animal research at National Cardiovascular Center. Each animal underwent two [11C] raclopride PET scans under anesthetic state, one for after rTMS and the other for after sham-sound stimulated control condition, with a 2-week interval. The orders of two conditions were counterbalanced among subjects. For the rTMS condition, rTMS consisted of 20 trains of 5Hz rTMS stimulation for 20 sec with an inter-train interval of 40 sec using a small-sized eight-figured coil dedicated for stimulation of *macaca fascicularis*. The strength of the TMS stimulation was set to 35% of maximum of stimulator, which was determined by a plastic cranium phantom for *macaca fascicularis* . The coil was positioned to be centered on the target site to the right M1 cortex 20 mm lateral to midline (corresponding to upper limb region), which was determined from corresponding T1-weghted MR images, obtained by the inversion recovery, FSPGR sequence (TR=9.4msec, TE=2.1 msec, TI=600msec) using a 3-Tesla MR imager (Signa LX VAH/I, GE, Milwaukee, USA) under pentobarbital anesthesia. For control condition, sham-sound stimulation consisted of sequential sounds of rTMS, which was sampled from rTMS

stimulation and was performed using a set of stereo-sound speaker placed near the animal head. PET scan was started 5 min after the finish of each stimulation

PET scan

Scans were performed on the ECAT EXACT HR PET scanner (Siemens-CTI, Knoxville, USA) at Bio-Functional Research Institute at National Cardiovascular Center. Anesthesia was induced with intra-muscular injection of ketamine hydrochloride (10mg/kg) and then maintained with continuous venous anesthetics, propofol and a muscle relaxant, vecuronium-bromide (0.25 mg/kg/hr). Animals were intubated with cuffed tracheal tube with 4.5 mm in inner diameter (Sheridan, Kendall Co., USA) and the respiration was controlled by anesthetic ventilator, Cato (Drager, Germany) with a 24%O2/76%N2 mixtured gas. Arterial and venous catheters were indwelled in femoral artery and antecubital vein, respectively. An anesthetic level was monitored using bispectral index (BIS) monitoring system (Aspect Medical Systems, USA) which enable to quantitate non-linear interrelations of single frequency components within the electroencephalography and the infusion rate of anesthetics (proporol) was controlled within a range of 3-6mg/kg/hr to obtain stable score of 87 as BIS index, corresponding to mile anesthetic level when used in human. BIS index has been shown to linearly correlate with cerebral glucose metabolism during propofol anesthesia (Alkire, 1998) and also useful for estimating anesthetic level in animals (Schmidt et al., 2000; Villa et al., 2000; Haga and Dolvik, 2002). The respiratory condition was monitored with end-tidal carbon dioxide level and intermittent arterial gas sampling and the ventilated volume was adjusted by altering a respiratory rate (10-15/min) or a tidal volume (65-85ml) to achieve normal blood gas condition (PaO2 95 mmHg, PaCO2 38 mmHg). Blood pressure, heart rate and body temperature were monitored during the experiment with a body heated with controlled heating blanket. After allowing waiting period of two hours to achieve physiologically stable state and to get withdrawal from the effect of ketamine, animals were positioned in the PET scanner with its head fixed in the molded polyurethane holder. A 15-minute transmission scan for attenuation correction was performed using with a rotating 68Ge/68Ga rod source. As biding potential for raclopride is varied in dependent on total injected mass (Lammertsma and Hume, 1996), a mass of 1 to 4 picomol/kg of [11C] raclopride was prepared by measuring a specific activity of the product (radioactivities of 166 – 370 MBq at 1 min prior to the injection) and the mass for each animal were adjusted as equal as possible between two PET scans. The solution of the tracer was injected intravenously over a minute period. Data acquisition began at the onset of the tracer injection and continued for 60 minutes in 39 time frames of gradually increasing individual durations (10 - 300 sec). For the justification of the coil position, the subsequent PET scans were performed after intra-dermal injection of radioactive tracer to the center of coil for TMS condition. PET

image of [11C] raclopride radioactivity was reconstructed by filtered back projection with a matrix of 128×128×47 and a voxel size of 1.1×1.1×3.13 mm.

Data analysis

Voxel-wise images were analyzed using statistical parametric mapping (SPM99; Welcome Department of Cognitive Neurology, London, UK). PET images were summed and co-registered to the subject's MRI using mutual information algorithm (Ashburner et al.,1997). Then T1-weighted MRI images were transformed to a standard brain space of macaca fascicularis (Martin and Bowden, 2000). This transformation was applied to co-registered PET images and parametric images of binding potential of C-11 raclopride. Binding potential (BP) of [11C] raclopride was estimated in a voxel-wise parametric image method, based on the simple reference tissue model (Lammertsma and Hume, 1996, Gunn et al., 1997). The normalized parametric images were then smoothed with isotropic Gaussian kernel (FWHM of 10 mm). The change of BP in rTMS and sham stimulation was tested by voxel by voxel paired t-test. Statistical inferences were based on the theory of random Gaussian field theory (Friston et al.,1995). Because of deviated distribution of [11C] raclopride, the statistical analysis was only performed on the striatum volume, as defined using a threshold mask obtained from a mean image of normalized [11C] raclopride images of all subjects. We performed volume of interest (VOI) analysis using MarsBar toolbox for SPM (http://www.mrc-cbu.cam.ac.uk/Imaging/marsbar.html) (Fig.1).

Results

Table 1 demonstrated physiological parameters (blood pressure, PaO2, PaCO2, BIS) during sham and rTMS experiments. There is no significant difference between sham and rTMS experiments in each parameter. Repetitive TMS of the right primary motor cortex (M1) of the hand area decreased [11C] raclopride BP in the bilateral ventral striatum including the nucleus accumbens (NAc) compared with rTMS of the sham condition (Fig.2). Such a change is most likely because of an increase in extracellular dopamine concentration in the ventral striatum after stimulation over the M1. On the other hand, increased [11C] raclopride BP in compared with rTMS of the sham condition was noted in the right putamen (Fig.3). Table 2 demonstrates BP values from the ventral striatum and the right posterior lateral part of putamen that were derived from a volume-of-interest drawn on the spatially normalized mean MRI of all subjects. Wilcoxon test revealed a significant ($p < 0.05$) effect of stimulation for the bilateral NAc and the right posterior lateral part of the putamen, but not for other striatal regions. The mean magnitude of change of the BP in the right NAc, left NAc and the right putamen were –8.12 %, –8.2 %, and 10.51 %, respectively.

Discussion

In this study, we found that rTMS over the left M1 can evoke release of dopamine in the ventral striatum including the nucleus accumbens (NAc) in anesthetized monkeys. No significant reduction of binding potential (BP) was found in the dorsal striatum but a significant increase of the BP in the right putamen was observed.

One superior point of this study is that we gave rTMS on anesthetized monkeys. Dynamic changes of the dopaminergic system, particularly the mesolimbic dopaminergic system, are susceptible to uncontrollable and /or subliminal mental status of subjects, e.g.; placebo effects and expectation for pay or rewards after experiments. For example, it is known that little activation in ventral striatum occurs when attention- or alertness-generating events such as aversive stimuli as revealed by alert monkey study (Mirenowics and Schultz 1996). Under anesthesia, such confounding effects should be negligible. Further, rTMS experiments on small animals such as rats have a technical problem whether given stimuli are localized at the stimulated area or spread onto large cortical areas. We consider that the experiment with anesthetized middle-sized animals such as monkeys should be ideal for the estimation of modulating effects of rTMS on the dopaminergic system without confounding factors mentioned above. There may be a controversy regarding generalized anesthesia performed in this study. One would argue that rTMS might induce alteration in the anaesthetic level and it might have served as confounding factor. However, we have estimated the anesthetic level by quantitative non-linear analysis of electroencephalography during rTMS and found no

significant difference from that during sham stimulation. Physiological parameters showed no changes during rTMS. We considered that observed changes in dopaminergic system should be independent of the effect of generalized anesthesia.

We will first discuss modulating effects on the mesolimbic and mesostriatal pathways by rTMS separately, and then discuss the possibility of rTMS treatment for Parkinson disease (PD).

Effects in the ventral striatum

The ventral striatum, particularly NAc, is a target of the mesolimbic dopamine system, which arises in dopaminergic neurons in the ventral tegmental area (VTA) (Oades and Halliday, 1987). These VTA neurons also innervate several other limbic structures such as amygdala and limbic regions of neocortex (Oades and Halliday, 1987). The NAc, and its dopaminergic inputs, play critical roles in rewards, reinforcement and incentive motivation. Experimental impairments in NAc lead to motivational deficits in approach behavior, reward-directed learning, and attentiaonal responses (Wise and Hoffman, 1992; Robins and Everitt, 1996). According to experiments in alert monkeys, the activity VTA neurons increases when positive rewards are received beyond previous expectation while it is reduced when an expected positive reward is omitted (Schultz et al., 1997). Several cognitive activation studies in human using [11C] raclopride PET also suggested that dopamine should be released in the ventral striatum during positive unpredicted rewards (Koepp MJ et al. 1998, Pappata S et al. 2002).

In pathological conditions, researches of the VTA-NAc pathway and of dopaminergic mechanisms have mainly focus on addiction. Recently, as well as serotonin and noradrenaline, alteration of the mesolimbic dopamine pathway have been suggested to be involved in the pathogenesis of some of the major symptoms of depression, a pervasive absence of behavioral incentive, such as apathy, anhedonia, amotivation (Nestler EJ et al. 2002). These suggest that activation of the ventral striatum by rTMS over M1 may make non-specific motivation higher and give beneficial effects on depression and motor symptoms.

Which pathways are used in this effect? One previous study of C-11 raclopride PET with rTMS over the left dorsolateral prefrontal cortex (DLPFC) in humans showed that the BP change was seen only in the ipsilateral head of the caudate nucleus (Strafella AP et al. 2001). Because of different parameters of rTMS, experimental design, conditions of subjects (anesthetized v/s awake) and species (monkey v/s human), direct comparison between our results and those of this study is difficult. However, one critical difference between two studies is whether the dopamine released striatal regions have direct anatomical and/or functional connections to the stimulated areas. Their study suggested that fibers originating from the DLPFC should be involved in promoting local dopamine release at their striatal target site. On

the other hand, our data demonstrated that the BP decrease was found in the ventral striatum, which have no direct projection from the stimulated area (M1). Motor and premotor areas project to the putamen centrally and caudally, whereas the ventral striatum receives its frontal input from the orbital and medial frontal cortex including anterior cingulated cortex (Haber et al., 2000). We consider that dopamine release in the ventral striatum could occur via direct and indirect connections between the motor cortex and midbrain dopamine neurons. Molina (1965) reported projections from the motor and premotor cortex of the cat to the VTA (Oades and Halliday, 1987). In rats, stimulation of the prefrontal cortex can promote widespread striatal dopamine release by activation of dopamine neurons in the VTA (Keck et al. 2002). Taken together, we suppose that rTMS over the M1 induces dopamine release in the ventral striatum through the VTA.

Effects in the dorsal striatum (the putamen)

We found increased BP in the putamen after rTMS. The result indicated that rTMS over the M1 deactivated the putamen. Because of rich connections between the putamen and the M1, it is likely that rTMS over the M1 can strongly modulate dopaminergic function in the putamen. On the other hand, disturbance of movement such as akinesia and bradykinesia in PD is associated with dysfunction dorsal striatal dopaminergic pathway. Therefore, our data indicated that rTMS over M1 might worsen motor symptoms due to deactivation of the dorsal striatal pathway in PD patients. Indeed, Boylan et al. (2001) reported that rTMS over the supplementary motor area worsened motor performance in PD patients.

Another interpretation for the increment of BP in the putamen is an apparent change of BP in consequence of increased regional blood flow (rCBF) in the putamen caused by rTMS. Several neuroimaging studies combined with rTMS have revealed that rTMS activated functionally connected distant areas as well as stimulated sites (Paus et al., 2001, Fox et al., 1997). Therefore, it is plausible that rTMS over the right M1 induce an increased rCBF in the putamen. The rCBF change could be a confounding factor in the detection of endogenous dopamine release measured by the C-11 raclopride PET study. Logan et al. (1994) showed that a rCBF decrease induced by hyperventilation resulted in a reduction of distribution volume (a parameter similar to the BP). Their data suggest that the BP increase in the putamen in the present study should reflect a rCBF increase rather than a reduction of endogenous dopamine release in the putamen. To clarify this issue, we are going to simultaneous measurement of C-11 raclopride PET and microdyalysis in the same experimental design.

rTMS treatment for PD

There are still controversies about the efficacy of rTMS on PD. Recently, Okabe et al. studied therapeutic effects of rTMS in PD patients with a realistic sham procedure and concluded that the low frequency rTMS has no more than placebo effect on PD symptoms,

suggesting importance to demarcate the benefits between sham and real stimulations (Okabe et al.,2003). With respect to PD, activation of the mesostriatal dopaminergic pathway is likely to be a possible candidate mechanism behind the therapeutic effects of rTMS on its motor symptoms. In contrast, our data suggested that rTMS over the M1 deactivated the mesostriatal dopaminergic pathway. However, if rTMS is effective in PD patients, we may explain their mechanism based on our present results. Depressive mental state is a common complication in Parkinson's disease (PD). Some PD patients suffer from anergia, anhedonia, apathy, and passivity that may be explained by the alteration of the mesolimbic dopaminergic system (Cummings JL 1992). In this context, we consider that modulating effects on the VTA-NAc pathway elicited by rTMS over M1 may improve concomitant depressive status in PD or make the motivation higher, and it is one of possible therapeutic mechanisms for rTMS treatment of PD. Furthermore, we assume that forced expectation induced by the activated mesolimbic dopaminergic pathway may cause strong placebo effects in PD patients. In PD, the placebo effect can be prominent. Recently, de la Fuente-Fernandez et al. (2001) reported that substantial release of endogenous dopamine in dorsal striatum of PD patients in response to placebo. Such a fact supports our notion.

In contrast, deactivation of the putamen would have a possibility of negative effects on the motor symptoms. Because of technical issue of BP measurement using PET, we can not conclude rTMS over the M1 reduces dopamine release in the putamen at this point. We suppose the final outcome of rTMS on PD should be a summation of these two effects; non-specific increased motivation (the mesolimbic system) and possible decreased motor performance (mesostriatal system), which must have much inter-individual variability.

Conclusions

Although, several issue remains to be clarified, our results suggest that therapeutic mechanisms of rTMS should be explained by the activation in the mesolimbic dopaminergic pathway.

Acknowledgment

This study was supported by Health Science Research Grant (H13-005) from the Ministry of Health, Labour and Welfare.